Peponi, L. et al., 2018. Thermally-activated shape memory effect on biodegradable nanocomposites based on PLA/PCL blend reinforced with hydroxyapatite. Polymer Degradation and Stability, 151, pp.36–51.

Thermally-activated shape memory effect on biodegradable nanocomposites based on PLA/PCL blend reinforced with hydroxyapatite

Laura Peponi[1]*, Valentina Sessini[1, 2], Marina P. Arrieta[1], Iván Navarro-Baena[1, 2], Agueda Sonseca[3], Franco Dominici[2], Enrique Gimenez[3], Luigi Torre[2], Agnieszka Tercjak[4], Daniel López[1] and José M. Kenny[2]

[1] Instituto de Ciencia y Tecnología de Polímeros, ICTP-CSIC., calle Juan de la Cierva 3, 28006, Madrid, Spain. lpeponi@ictp.csic.es, v.sessini@ictp.csic.es, marrieta@ictp.csic.es, daniel@ictp.csic.es,

[2] Dipartimento di Ingegneria Civile e Ambientale, Università di Perugia, Strada di Pentima, 05100 Terni, Italy. ivan.navarrobaena@gmail.com, francodominici1@gmail.com, luigi.torre@unipg.it, jose.kenny@unipg.it

[3] Instituto de Tecnología de Materiales, Universitat Politècnica de València (UPV), Camino de Vera s/no, Valencia, Spain. enrique.gimenez@mcm.upv.es, agsonol@posgrado.upv.es

[4] Group Materials + Technologies (GMT), Department of Chemical and Environmental Engineering, Polytechnic School, University of the Basque Country (UPV/EHU), Plaza Europa 1, Donostia-San Sebastián, Spain. agnieszka.tercjaks@ehu.es

* Corresponding authors: Laura Peponi – lpeponi@ictp.csic.es
ICTP-CSIC, calle Juan de la Cierva, 3, 28006 Madrid.
tel: +34 91 258 74 24; Fax: +34 91 564 48 53

ABSTRACT

In this work, the effect of the addition of different amount of nanosized hydroxyapatite (nHA) on the shape memory behaviour of blends based on poly(lactic acid) (PLA) and poly(ε-caprolactone) (PCL) has been studied. In particular PLA/PCL blend with 70 wt % PLA has been reinforced with 0.5, 1 and 3 wt % nHA. Moreover, the relationship

between the morphology and the final properties of the nanocomposites has been investigated by field emission scanning electron microscopy, confocal Raman spectroscopy and atomic force microscopy. In particular, PeakForce has been used to study quantitative nanomechanical properties of the multifunctional materials leading to conclusion that nHA increase the phase separation between PLA and PCL as well as act as reinforcements for the PCL-rich phase of the nanocomposites. Furthermore, excellent thermally-activated shape memory response has been obtained for all the nanocomposites at 55 ºC. Finally, the disintegration under composting conditions at laboratory scale level was studied in order to confirm the biodegradable character of these nanocomposites. Indeed, these materials are able to be used for biomedical issues as well as for packaging applications where both thermally-activated shape memory effect and biodegradability are requested.

Keywords: Biodegradable blends, PLA, PCL, nanocomposites, nanosized hydroxyapatite, shape memory.

1. Introduction

In recent years the interest of new kinds of biodegradable nanocomposites to be used in different applications fields, is strongly increased [1-3]. Among them, nanocomposites based on biopolymers are focusing the attention of both scientists and industry, looking for new environmental-friendly materials [4].

Moreover, the combination of biodegradable materials by melt blending approach at lab scale presents many advantages because it offers the opportunity to tune their physical properties over a wide range through a relatively simple, cost effective and readily available processing technology easily scalable at industrial level [5].

Biopolymers such as poly(lactic acid) (PLA) and poly(ε-caprolactone) (PCL) have been widely studied for a wide number of applications, in particular in the biomedical sector [6, 7] and for short term applications (i.e. packaging, agricultural mulch films, etc.) [8]. Both polymers are aliphatic polyesters, biocompatible and biodegradable. In addition, PLA can be obtained from renewable resources. They have very interesting properties by themselves, but their combination allows obtaining new materials with unique properties through their copolymerization [9] as well as by blending [10] them. In fact,

starting from PLA-b-PCL block copolymer structures as well as from their blends, materials with enhanced mechanical response, showing different thermal behavior, with tunable degradation rate or even smart materials with shape memory behavior have been designed [11-15].

PLA and PCL are not miscible, so their blend is characterized by a phase separation, which plays a very important role in their final properties [16]. Ferri et al. [10] blended PLA with PCL as flexible polymer in different proportion to improve ductile properties of PLA. They observed a lack of miscibility. However, their results showed that the addition of 20-30 wt % of PCL provides attractive ductile properties to PLA. In our previous work, immiscible PLA/PCL blends were also prepared using different PLA:PCL composition, 100:0 70:30, 50:50, 30:70 and 0:100 confirming the possibility to design PLA/PCL blends with desired mechanical performance [17]. Moreover, the presence of two different phases is particularly important when working with shape memory materials. In fact, shape memory is the capability of a material to change its shape in a temporary one and to recover its initial shape when an external stimulus is applied [18]. Different stimuli are able to promote the shape memory response such as temperature, light and humidity, among others [19-20]. However, the presence of two different phases is required thus taking into account that one acts as fix phase, able to recover the initial shape and the other one is the switching phase, characterized by a particular transition temperature (T_{trans}) that allow to fix the temporary shape [21]. In order to study the thermally-activated shape memory behaviour, thermo-mechanical cycles can be performed. Once identified the T_{trans} of the switching phase, during the programming stage, the sample is able to fix its temporary stage applying the temperature as external stimulus, and then, during the recovery stage, the sample recovers its initials shape when the external stimulus is applied. Two are the main parameters to be studied when working with the shape memory materials, the strain fixity ratio (R_f) and the strain recovery ratio (R_r), indicating the ability to fix the temporary shape and to recover the initial shape, respectively [22].

Dong et al. [23] reported a pioneering work on shape-memory material based on PLLA/PCL blends in 2011. They reported that PLLA/PCL blend with the weight ratio of 1:3 presents a R_r of about 95% within 22s.

In our previous work we found that PLA/PCL blend with 30 wt % of PCL is able to present thermally-activated shape memory behavior at 55 ºC [17]. Therefore, in this

paper the effect of the addition of nanoreinforcements on the shape memory behavior of this blend was studied thus considering that well dispersed nanoreinforcements can improve the properties of the neat polymeric matrix and at the same time can modify the compatibility between the different polymeric phases [24, 25] changing its shape memory response as well as can affect to the transition temperature required for the thermally-activated shape memory effect. At this regard Navarro-Baena et al. [26] reported that the incorporation of cellulose nanocrystals in a poly(ester-urethane), based on PLA and PCL, enhances the shape memory response, obtaining a R_f value of about 90 % for the bionanocomposite, much better than the value of 70 % reported for the neat matrix. However, they reported that the transition temperature for the neat polymeric matrix is slightly different that the one used for the bionanocomposites as a consequence of the addition of nanofillers.

Therefore, nowadays, to study the effect of the incorporation of nanofillers in shape memory systems is a very important challenge to be deeply explored. Very few works are reported in the literature about these smart nanoreinforced systems evidencing the difficult to obtain very-well optimized smart nanocomposites. Recently, Molavi et al. [27] reported an interesting study on triple shape memory behaviour of nanocomposites based on blends of PLA and PCL reinforced with graphene nanoplatelets.

However, based on our knowledge, at this time, no work on shape memory response of PLA/PCL blends reinforced with hydroxyapatite (HA) have been yet published.

Among nanofillers, hydroxyapatite at its nano-level, nano-hydroxyapatite (nHA), is widely used as reinforcement thus considering that it is the most relevant mineral component of human hard tissues [28]. Moreover, electrospun PLA fibers reinforced with nHA are able to increase the storage modulus [29]. On the contrary, the addition of nHA does not affect significantly the thermal behavior of the polymeric matrix. For instance, Kaur et al. [30] studied the thermal properties of PCL, finding that they are not significantly affected by the presence of hydroxyapatite, while the crystallinity slightly decreases. We recently observed that nHA increased the size of the meso-structured domains in a poly(ester-urethane) nanocomposites due to the increased interaction of the HA nanofillers with the separated poly(ester-urethane) domains [31]. Additionally, depending on the nHA amount, a plasticizing effect (0.5 and 1 wt %) or a reinforcement effect (3 wt %) can be produced [31]. Moreover, introducing small amount of nHA to the polymeric matrix, it is possible to obtain a more hydrophilic material [31].

In the present work, shape memory response of biodegradable PLA/PCL blend reinforced with nanosized hydroxyapatite at three different contents (0.5, 1 and 3 wt %) has been studied. A morphological and structural characterization of the processed materials have been performed with different techniques, such as scanning electron microscopy (SEM), Fourier transformed infrared spectroscopy (FTIR), Raman spectroscopy in mapping mode and atomic force microscopy (AFM). Moreover, a comprehensive analysis was performed with AFM in terms of changes in mechanical properties induced by the presence of nHA using PeakForce quantitative nanomechanical property mapping (QNM). Their thermal and mechanical properties were also studied and correlated with their structural and morphological characterization. Therefore, thermally-activated shape memory properties were studied by dynamic mechanical thermal analysis (DMTA) focusing the attention on the effects of the addition of nHA on the shape memory behaviour of the PLA/PCL blend in term of both strain recovery and strain fixity ratios. Finally, the disintegration under composting conditions at laboratory scale level was performed to confirm the biodegradable nature of these nanocomposites. The disintegration levels were evaluated by monitoring the nanocomposites weight loss, while morphological and structural changes were followed by SEM and FTIR, respectively.

2. Experimental

2.1 Materials

PLA 3051D (D-lactide content of 4%) with density of 1.25 g/cm^3 and a molecular weight (M_n) of about 1.42 × 10^4 g/mol, was supplied by Nature Works®, USA. PCL CAPA8000 was kindly donated by Perstorp. Non-commercial nanosized hydroxyapatite, synthesized by chemical precipitation method [29], were used as nanofillers. In brief, calcium hydroxide ($Ca(OH)_2$) was dissolved in an aqueous solution of gelatin, this solution was then appended drop by drop to an aqueous solution of ortho-phosphoric acid (H_3PO_4, 85 %) in order to obtain a stoichiometric hydroxyapatite, with a ratio of calcium and phosphorous (Ca/P) of 1.67 moles. The solution was basified until pH 10 using and the precipitated nHA showed a particle size of about 35 nm.

2.2 Processing of polymeric blends and their bionanocomposites

PLA was blended with 30 wt % of PCL and further loaded with 0.5, 1 and 3 wt % of nHA by extrusion. Prior to processing, all the materials were dried in an oven at 40 °C under vacuum during 24 h. The samples were prepared in a DSM Xplore co-rotating extruder at a screw speed of 100 rpm for 3 min at 180 ºC. Then, the materials were compressed into films of 500 μm using a Dr. Collin 200mm x 200mm press at 180 °C. First, the extruded materials were heated for 1 min at atmospheric pressure and then 50 bar of pressure were applied for 1 min. The obtained films were cooled to room temperature with water-refrigerated aluminium plates under a pressure of 50 bar. The obtained materials were named as M70PLA for the neat blend, M70PLA0.5HA, M70PLA1HA and M70PLA3HA for the three different nanocomposites, thus emphasizing the respective nHA content.

2.3 Characterization techniques

Field emission scanning electron microscope (FE-SEM, Hitachi S8000) in transmission mode was used to study the morphology of the nanosized hydroxyapatite as well as its dispersion in the polymeric matrix. The morphology of the PLA/PCL blend and its nanocomposites was investigated by scanning electron microscopy (SEM PHILIPS XL30 with a tungsten filament). The polymeric samples were frozen under liquid N_2 and then cryo-fractured. All the samples were gold/palladium coated by an automatic sputter coated Polaron SC7640.

Atomic force microscopy (AFM) analysis was performed operating in tapping mode with a scanning probe microscope (Nanoscope IIIa, Multimode TM from Digital Instruments and Nanoscope V, Dimension Icon form Bruker). Samples were cut using an ultra-microtome Leica Ultracut R with a diamond blade. Height and phase images were obtained under ambient conditions with typical scan speed of 0.5-1 line/s, using a scan head with a maximum range of 16 μm x 16 μm. AFM also has been used for a quantitative nanomechanical (QNM) analysis. Measurements were carried out using PeakForce mode under ambient conditions. Commercial reflective Al tips (TAP150A with a resonance frequency of ~150 KHz) were used. The measurements have been performed with a calibrated optical sensitivity, the exact spring constant was calculated

using the Thermal Tune option and a defined tip radius was adjusted using PS as standard.

The structural characterization was also conducted by FTIR measurements which were carried out in transmission mode in the 4000-650 cm^{-1} spectra region at room temperature (resolution of 4 cm^{-1} and 32 scans) with a Spectrum One FTIR spectrometer (Perkin Elmer instruments).

Raman mapping measurements were performed in order to study the morphology of the samples [32] by mean of a Renishaw *In Via* Reflex Raman Microscope (Wotton-Under-Edge, UK). An optical microscope is coupled to the system. The laser beam is focused on the sample with an Olympus 0.75 × 50 microscope objective. The spatial resolution was about 1.22 μm. Calibration was done by referring to the 520 cm^{-1} line of silicon. The Raman scattering was excited using a diode laser at a wavelength of 785 nm (320 mW power). An automatic motorized translator X-Y stage was used to collect two dimensions images. A total of 960 spectra was recorded at the interval of 800 cm^{-1} and 1150 cm^{-1} in order to mapping the different areas, thus considering the vibration band of PLA at 873 cm^{-1} and the skeletal stretching for PCL at 1109 cm^{-1}.

Thermal properties were investigated by differential scanning calorimetry (DSC) analysis using a Mettler Toledo DSC822e instrument. Samples of about 10 mg were sealed in aluminum pans. Thermal experiments were composed by three cycles: firstly a heating scan, from 25 ºC to 200 ºC, then a cooling scan from 200 ºC to -90 ºC and finally a heating scan from -90 ºC to 200 ºC. All the scans were performed with a heating rate of 10 °C/min run under nitrogen purge. The melting temperatures (T_m) and the melting enthalpy (ΔH_m) were obtained from the first heating scans. Moreover, thus considering that no further thermal treatments occur on the samples in order to study their thermally-activated shape memory response, the first cycle is use to choose the parameters for the shape memory analysis. The degree of crystallinity of the samples was calculated according with Equation 1.

$$\chi_c^a = \frac{1}{1-X^a}\left[\frac{\Delta H_m}{\Delta H_{m0}}\right] \cdot 100 \qquad \text{Equation 1}$$

where ΔH_{m0} is the melting enthalpy for a 100 % crystalline material and X^a is the percentage of the crystalline component *a* in the sample. The value taken for ΔH_{m0} of PCL was 148 $KJ \cdot mol^{-1}$, while for PLLA was 93 $KJ \cdot mol^{-1}$ [33].

The mechanical properties were determined using an Instron Universal Testing Machine at a strain rate of 200 mm/min according to ISO 37:2011 [34]. Measurements were performed on 5 dog-bone specimens with a width of 2 mm and leaving an initial length between the clamps of 20 mm. From these experiments were obtained the Young modulus, as the slope of the curve between 0 % and 2 % of deformation, the elongation at break and the maximum strain reached.

Dynamic mechanical thermal analysis (DMTA) of the samples was carried out using a DMA Q800 from TA Instrument in film tension mode with an amplitude of 5 μm, a frequency of 1 Hz, a force track of 125 %, and a heating rate of 2 ºC/min. Samples subjected to DMTA were cut from compression-moulded films into regular specimens of approximately 20 mm × 5 mm × 0.60 mm.

Thermally-activated shape memory characterization was performed by thermo-mechanical cycles by DMTA at a T_{trans} closed to the T_m of PCL thus considering that in our system, PLA acts as fix phase while crystalline PCL is the switching phase. In fact, in order to perform thermally-activated shape memory analysis, it is necessary to heat the sample above the corresponding T_{trans} and to strain the sample to a desired shape. Then, the material is cooled while maintaining the deformation. Once the applied stress is removed, the recovery of the original shape occurs by re-heating the sample above the T_{trans}. Therefore, in order to analyse the effects of the addition of nHA on the thermally-activated shape memory response of the PLA/PCL blend, a deformation of 50 % (ε_m) has been used. The samples were heated at a temperature of 55 ºC, for 5 min, and stretched until ε_m is reached by applying a constant deformation stress. They were then quenched at 0 ºC under the same constant stress. The temporary shape, was recovered after releasing the stress, and the permanent shape, characterized by an elongation of ε_p, was recovered upon heating (3 ºC/min) to 55 ºC. Three different thermo-mechanical cycles have been performed for each material. Moreover, with the aim to get a quantitative estimation of the thermally-activated shape memory properties of the materials, the strain fixity ratio and the strain recovery ratio have been calculated. In particular, R_r, the ability to recover the initial shape, was taken as the ratio of the recovered strain to the total strain, as given by the following equation:

$$R_r(N) = \frac{\left(\varepsilon_m - \varepsilon_p(N)\right)}{\varepsilon_m - \varepsilon_p(N-1)} \times 100\ \% \qquad \text{Equation 2}$$

R_f, the ability to fix the temporary shape, is the ratio of the fixed strain to the total strain, as presented by the equation 3:

$$R_f(N) = \frac{\varepsilon_u(N)}{\varepsilon_m} \times 100\ \% \qquad \text{Equation 3}$$

where, ε_m is the deformed strain, ε_u the fixed strain, ε_p the recovered strain and N is the number of cycles.

The disintegrability test under composting conditions was performed at laboratory scale level following the ISO 20200 standard [35]. The nanocomposite films (15 mm × 15 mm) were contained in a textile mesh to allow their easy removal after composting test, but also allowing the access of moisture and microorganisms. They were buried at 4-6 cm depth in perforated plastic boxes containing a solid synthetic wet waste (10 % of compost (Compo, Spain), 30 % rabbit food, 10 % starch, 5 % sugar, 4 % corn oil, 1 % urea, 40 % sawdust and approximately 50 wt % of water content) and they were incubated at aerobic conditions (58 ºC). Each nanocomposite was recovered at 1, 17, 22, 38, 56 and 89 days of the composting test. The film samples were cleaned with distilled water, dried in an oven at 37 ºC during 24 h and reweighed. The disintegration degree was calculated by normalizing the sample weight, at different days of incubation, to the initial weight. In order to determinate the time at which 50 % of each nanocomposite was disintegrated, disintegrability degree values were then fitted using the Boltzmann Equation [36] with OriginPro 8.1 software as follows:

$$m = \frac{(m_i - m_\infty)}{1 + e^{(1 - t_{50}/d_t)}} \qquad \text{Equation 4}$$

where m_i and m_∞ are the initial and final mass values measured respectively at the beginning of the exposition to compost and after the final asymptotes of the disintegrability test. t_{50} is the time at which the materials disintegrability reaches the average value between m_i and m_∞, known as the half-maximal degradation and d_t is a parameter that describes the shape of the curve between the upper and lower asymptotes [36]. A qualitative check of the physical disintegration in compost as a function of time was also done by taken photographs, while the morphological and structural changes were followed by SEM observations as well as by FTIR measurements.

3. Results and Discussion

In order to analyze the effect of the addition of different amount of nHA on the thermally-activated shape memory behaviour of PLA/PCL blend, first of all both

thermal and mechanical characterization have to be performed in order to define the parameters for the shape memory analysis. At this regard, DSC analysis and TGA have been performed. The first heating scan of the DSC experiments is presented in **Fig. 1.a**. In our previous work [17], the T_g and T_m of neat PLA was found to be around 60 ºC and 150 ºC, respectively while those of PCL were of -63 and 58 ºC, respectively. T_m of both PCL and PLA homopolymers are not affected neither in their blend composition nor in the final nanocomposites. All the PLA/PCL nanocomposites present the characteristic PCL melting temperature at about 60 ºC. All the materials also showed PLA cold crystallization followed by the melting of PLA crystals. Even not shown, the T_g of PLA remains quite constant at 60 ºC, for all the materials studied. As it is shown in the **Fig. 1.a**, the nHA addition does not change significantly the thermograms of the first scan for the nanocomposites.

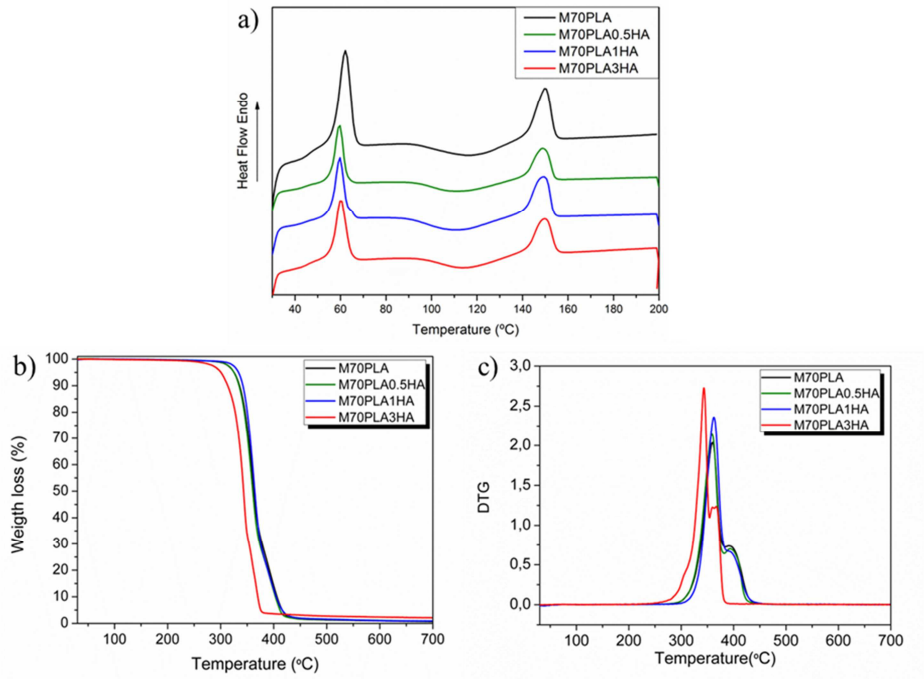

Samples		PLA	PCL
	$T_{5\%}$ (°C)	T_{max} (°C)	T_{max} (°C)
M70PLA	325	359	395
M70PLA0.5HA	325	359	395
M70PLA1HA	334	362	396
M70PLA3HA	300	343	359/366

Fig. 1. PLA/PCL blend and its nanocomposites: a) DSC 1st heating scan, b) TGA and c) DTG.

Indeed, the T_m and the X_c of both components of this blend, PCL and PLA, as well as for their nanocomposites did not change significantly as can be easily noted in the values summarized on Table 1.

Table 1. Melting temperature and degree of crystallinity for the different formulations.

	PCL		PLA	
	T_m (ºC)	X_c (%)	T_m (ºC)	X_c (%)
M70PLA	62	47	150	1
M70PLA0.5HA	60	40	149	3
M70PLA1HA	60	37	149	1
M70PLA3HA	60	44	150	4

Similar results were reported by Kesenci et al. for two different PLA loaded with high amounts of nHA where they testified no significant changes on the thermal properties [37]. A similar effect was described by Leung et al. [38] for PCL-based composites and nanocomposites filled with micro and nano hydroxyapatite, respectively, with large amounts of nanofillers, ranging from 5 % up to 40 %. They attributed these effects to the poor interface between the nanofiller and the PCL matrix. On the other hand, all investigated nanocomposites show a crystalline PCL phase. This result is in very good agreement with the possibility to use the PCL crystals as switching phase in order to study their thermally-activated shape memory response.

The thermal decomposition of M70PLA and its nanocomposites was studied by thermogravimetric measurements. The TGA and DTG curves are shown in **Fig. 1.b** and **Fig. 1.c**, respectively. In our previous work [17], we studied the thermal stability of PLA, PCL as well as PLA/PCL blends at different proportions. Precisely, $T_{5\%}$ was found to be at 312 ºC and 355 ºC for PLA and PCL, respectively, while the maximum degradation temperature was found to be at 355 ºC and 393 ºC on the same order. M70PLA blend and its nanocomposites degraded in two-steps (**Fig. 1.c**) with the first peak corresponding to the PLA thermal decomposition, and the second one related with the PCL degradation, as it was previously reported by us for PLA/PCL neat blends [17]. The $T_{5\%}$ and T_{max} of M70PLA were the same of neat PLA, indicating that the thermal stability of PLA did not change after the melt-blending process. In the case of nanocomposites, the addition of the lowest amount of nHA (0.5 wt %) did not produce significant changes on the thermal degradation process of M70PLA0.5HA with respect

to the neat M70PLA. Moreover, higher amounts of nHA (1 wt %) shifted the $T_{5\%}$ of PLA-rich phase in M70PLA1HA around 10 ºC to higher values, improving the thermal degradation of the PLA/PCL blend. Slight shifts to higher values were also observed for the maximum degradation temperatures of both PLA and PCL phases, even if these improvements were not significant. However, the addition of 3 wt % resulted in a decrease of the $T_{5\%}$ of about 25 ºC towards lowers temperature and also the T_{max} of both PLA and PCL decreased compared to the neat blend. This can be related to some aggregates of nHA for this nanocomposite. Moreover, for M70PLA3HA, occurs the most evident decrease of the T_{max} shifting this value approximately 30 ºC to lower values for the PCL phase and about 15 ºC for the PLA one. Nevertheless, it should be highlighted that there was no degradation at temperatures below 200 ºC which is the highest temperature used during the processing.

These findings were corroborated by means of FTIR measurements in the 1900-1300 cm^{-1} region of the spectra (**Fig. 2**).

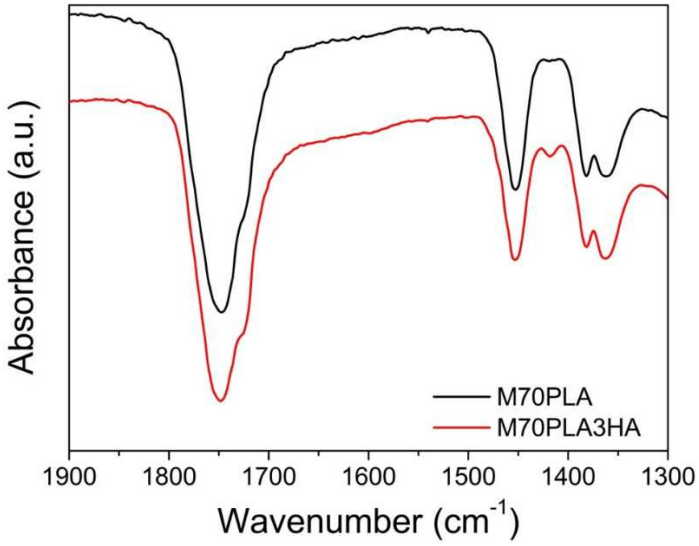

Fig. 2. Infrared spectra (1900-1300 cm^{-1}) of M70PLA and M70PLA3HA.

M70PLA and M70PLA3HA nanocomposites revealed the typical band at 1748 cm^{-1} assigned to the asymmetric stretching of the carbonyl group of lactides [8], which is overlapped with crystalline C=O stretching vibration of PCL that is assigned to the shoulder at 1722 cm^{-1}. At 1417 cm^{-1} appears a small peak in nHA based nanocomposites which is related to OH- bonds in nHA [39]. These may be an evidence of intermolecular interaction between OH- groups of nHA and carbonyl group of PCL confirming hydrogen bond interactions [40].

The mechanical response of the investigated nanocomposites was studied by tensile test experiments and the results are reported in **Fig. 3**. From the stress-strain curves of M70PLA blend and its nanocomposites (**Fig. 3.a**) it is possible to observe that all the samples show yield deformation at lower strains, characteristic of plastic deformation, as well as the strain hardening at higher deformation values before the sample breaks.

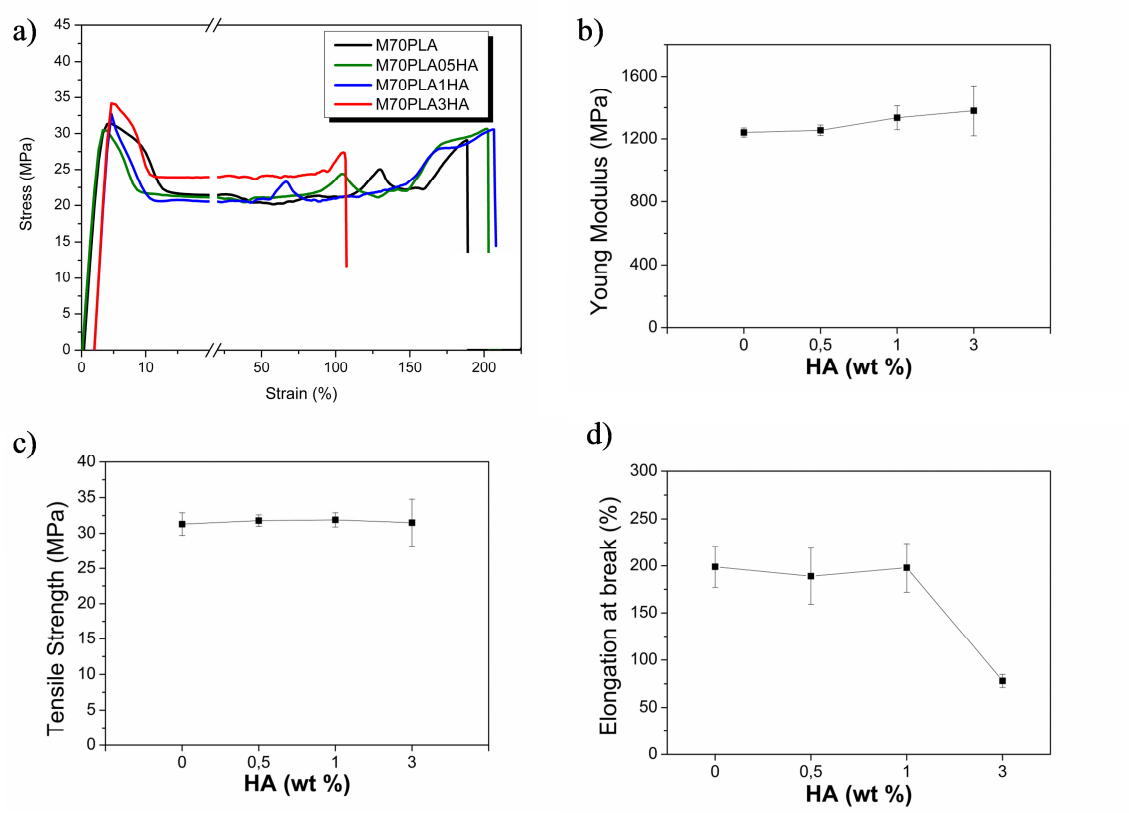

Fig. 3. Tensile test results of M70PLA blends and their bionanocomposites: a) stress-strain curves, b) Young modulus, c) tensile strength and d) elongation at break.

The addition of nHA produced an increase of the Young modulus (**Fig. 3.b**), while the tensile strength remains quite constant (**Fig. 3.c**) for all investigated nanocomposites. These small improvements can be attributed to the reinforcing effect of nHA into the polymer matrix. M70PLA blend reached elongations at break up to 200 % (**Fig. 3.d**) due to the plasticizing effect of PCL on PLA/PCL matrix, as previously reported [10, 17] and this values were maintained for the nanocomposites up to 1 wt % of nHA, while the stretchability strongly decreased for the highest amount of nHA (3 wt %). Similarly, for polyurethane nanocomposites based on PLA-b-PCL block co-polymer reinforced with small amount of nHA it has been observed that at least 3 wt % of nHA is required to reach the reinforcement effect of this nanofillers [31].

However, before to study the thermally-activated shape memory response of these materials, the main thermo-mechanical relaxations of the PLA/PCL blend and its nanocomposites were studied by DMTA and compared with both pure PCL and PLA. The evolution of the storage modulus (E'), loss modulus (E'') as a function of temperature are presented in **Fig. 4**.

The DMTA was performed from -100 ºC to 120 ºC for all the materials.

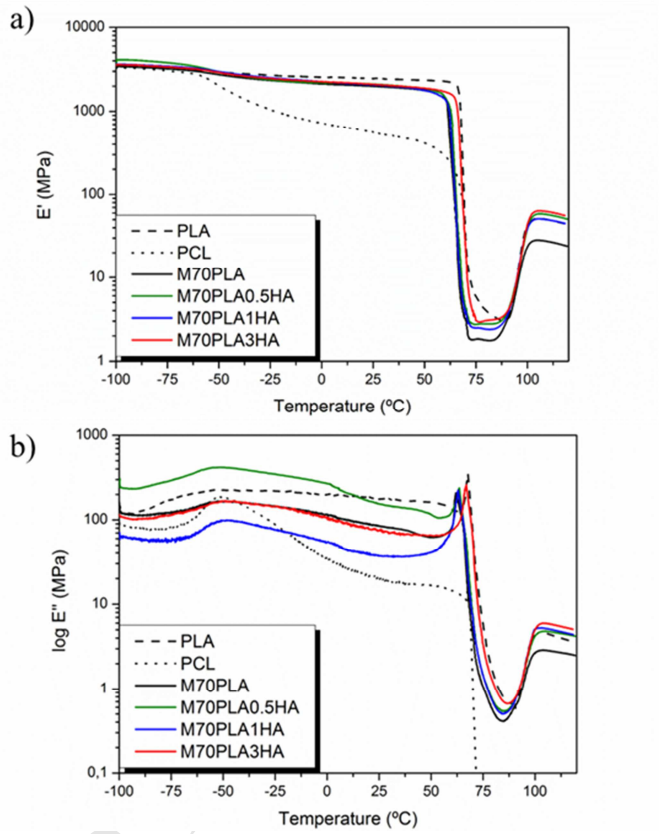

Fig. 4. Dynamic mechanical thermal analysis, a) storage modulus, b) loss modulus for all the investigated materials.

Regarding the storage modulus evolution (**Fig. 4.a**), all the investigated materials present a drop of the storage modulus in two steps, due to the T_g of PCL first and then the T_g of PLA. The addition of nHA to the blend provokes an increase on the storage modulus values in the glass state. Indeed, the higher values was reported for M70PLA0.5HA of about 4100 MPa while for the neat blend the value was 3400 MPa. For M70PLA1HA and M70PLA3HA the storage modulus is about 3600 MPa. The value of the storage modulus in the rubbery state (after 60 ºC) was about 100 MPa for all the investigated materials, followed by an increase of that value due to the cold crystallization of PLA. The loss modulus evolution (**Fig. 4.b**) shows the T_g relaxation

for both pure polymers, PCL and PLA, at -51 and 67 ºC, respectively. In the case of the neat blend, no changes were observed in the T_g values of PCL, although the T_g peak became broader while a slight decrease was shown for the PLA T_g (63 ºC). By the way, when the nHA was added into the blend, it is worth to note that the T_g of PCL was not affected by the filler addition. However, the T_g of PLA increases for M70PLA3HA, comparing with the neat blend and the other nanocomposites, reaching the same values as pure PLA.

Moreover, the morphology of pristine nHA as well as its dispersion into the polymer matrix was studied by FE-SEM in transmission mode, before to perform the thermally-activated shape memory analysis, as reported in **Fig. 5**. The nHA particles present a nanoroad-like morphology [41] and they show a wide dispersion of dimension in length but the thickness of these particles was measured to be around 35 nm. It is easy to notice the good dispersion of the nHA in the polymer matrix but increasing the nHA content the presence of very small aggregates was observed. Thus taking into account that it is difficult to understand the macroscopic behaviour of a material without understanding its microscopic structure, a deep study on the morphology of the phase separation of the neat blend and its nanocomposites has been carried out. In fact, when working with two polymeric systems, it is very important to study their morphologies in order to understand their final properties thus considering that phase separation is a key-factor to understand the macroscopic properties of polymeric blends as well as of copolymer systems [25, 42-46].

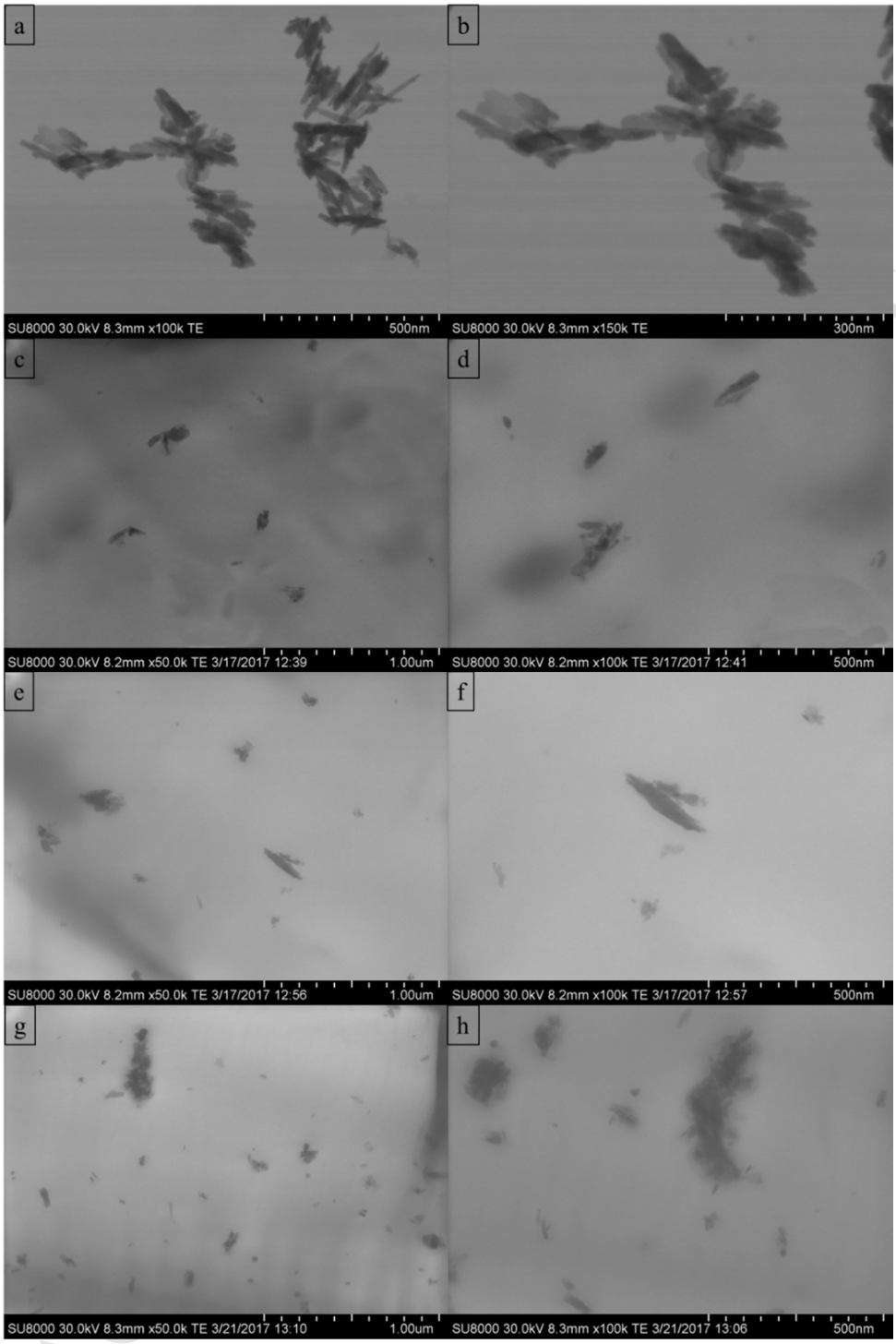

Fig. 5. FE-SEM images in transmission mode a-b) pristine nHA (100000x and 150000x), c-d) M70PLA0.5HA, e-f) M70PLA1HA and g-h) M70PLA3HA at two different magnitudes, 50000x and 100000x.

Therefore, the phase morphology of the fracture surface of the blend M70PLA and its nanocomposites was investigated by SEM analysis after their cryo-fractures. The images of the different samples are presented in **Fig. 6**.

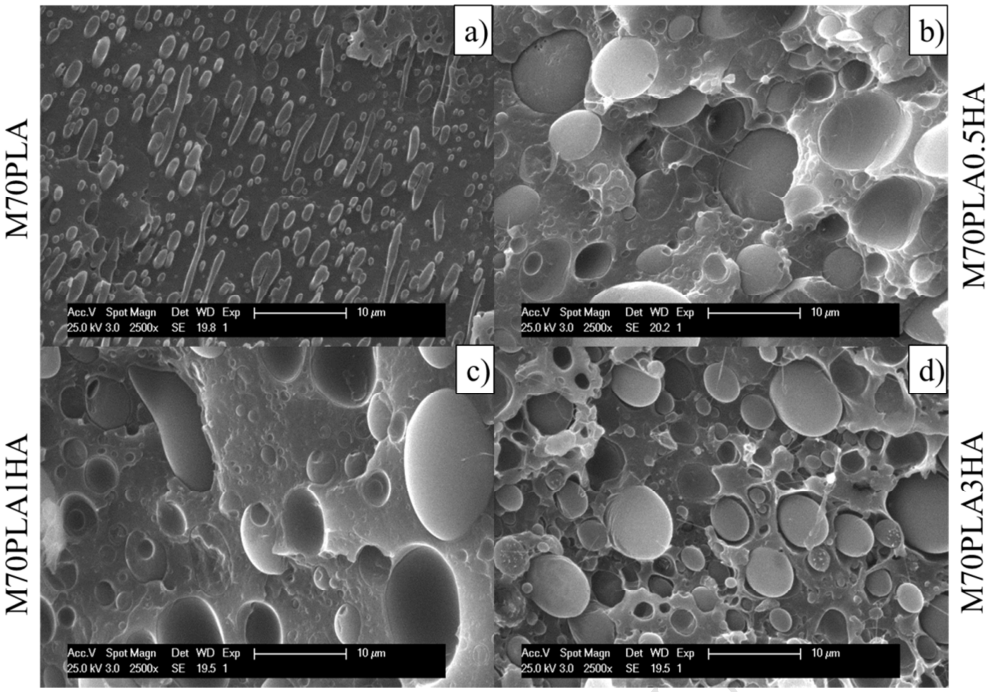

Fig. 6. SEM images (2500x) of PLA/PCL blend and its nanocomposites.

Clearly, all the samples show typical "island" morphologies, where small PCL spheres are dispersed in the PLA matrix, thus indicating poor adhesion between both polymers, which confirms their strong incompatibility as previously reported [17]. Meanwhile, the SEM images show that the addition of nHA strongly affect the morphology of the nanocomposites. From an irregular "ellipsoid-like drop" to a more spherical distribution of the PCL phase. The diameter of the PCL spheres increase according with the addition of the different amount of nHA in the nanocomposites. Although the size distribution for the PCL separated phase is very irregular when 0.5% nHA was added, for the M70PLA3HA, the PCL spheres were much ordered and smaller if compared with the other nanocomposites. In fact, by using a free software, Image J, it is possible to calculate the size of the PCL separated phase. For M70PLA it ranges from 300 nm to 5 µm, while the size of the PCL spheres in the nanocomposites varies from 300 nm to 40 µm, depending on the amount of nHA. This fact confirms that the addition of nHA changes completely the morphology of the blend, increasing the phase separation between PLA and PCL. Moreover, in the nanocomposite formulations some "empty" interface between the two polymeric phases is clearly presented, confirming their poor interfacial adhesion.

Confocal Raman spectroscopy was used in order to confirm the phase separation of the blend and its nanocomposites. In fact, this technique can be considered as a good

method to study both the phase separation and the distribution of the homopolymers in a polymeric blend and nanocomposites, allowing the identification of the different components [17]. In **Fig. 7** the Raman images as well as the Raman spectra for neat PLA/PCL blend and its nanocomposites are presented, evidencing the intensity of each signal. In particular, the green portion is related to the intensity of PCL signal from the band centered at 1109 cm^{-1}. The red region is related to the intensity of PLA signal, centered in the band at 873 cm^{-1} [17].

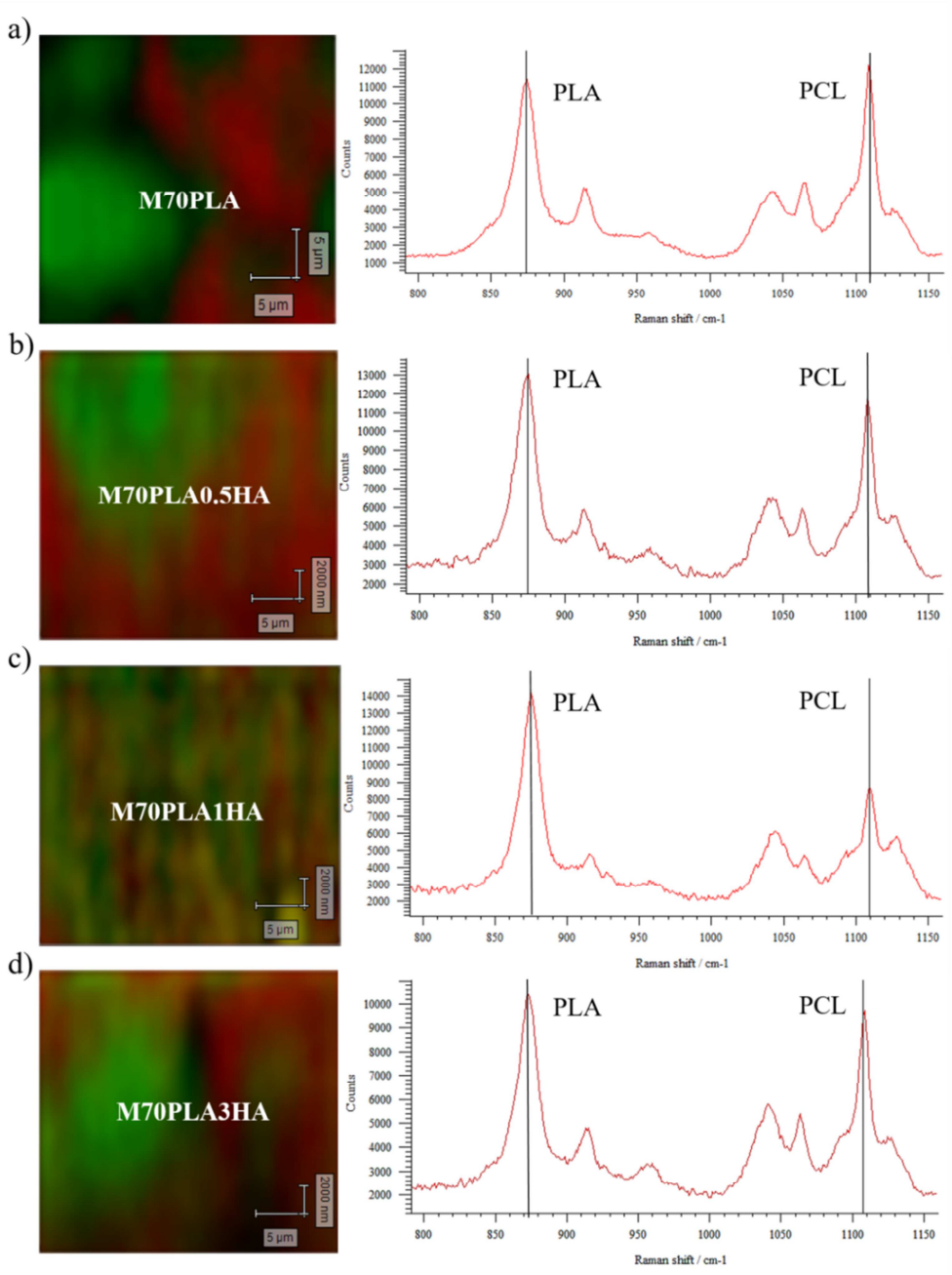

Fig. 7. Raman images with the corresponding Raman spectra of PLA/PCL blend and its nanocomposites.

From this analysis, it is evident that a phase-separated morphology clearly exists for the M70PLA blend and its nanocomposites, and it is possible to detect both the PLA-rich phase and the PCL-rich phase. In particular the dark regions of the Raman images (**Fig. 7**) correspond to the region in which both polymers exist, as can be confirmed also by Raman spectra in which both PLA and PCL centered bands have been obtained. For M70PLA can be appreciated that PLA forms a continuous phase (red regions of **Fig. 7**) with dispersed drops of PCL with different sizes (green regions of **Fig. 7**), confirming the morphology observed by SEM.

Regarding to the dark regions of the figures, which correspond to points with the contribution of both PCL and PLA homopolymer, M70PLA presents the largest ones, suggesting that between the polymers there was an interphase composed by both polymers, as previously reported [17]. For the nanocomposite, the dark region was almost disappeared indicating their morphological changes. This fact suggests that the presence of nHA decrease the "miscible interphase" between the two homopolymers leading to a worsening of the compatibility while the interfacial adhesion probably increase due to the physical interaction between the nHA and both homopolymers, as previously observed by FTIR analysis. Therefore, Raman maps are well related with the morphology previously obtained from the SEM images.

In order to study the morphological changes obtained when the nHA has been added to the polymer blends, mechanical studies has been also performed by AFM. The quantitative nanomechanical (QNM) properties of M70PLA and M70PLA3HA have been performed using a Dimension Icon Microscope equipped with a Nanoscope V controller from Bruker. In particular, in **Fig. 8** the AFM height images for the neat M70PLA blend and its nanocomposite with 3 wt % of nHA are reported. The AFM height images of both indicated that the addition of nanofillers changes the size of the separated domains of the PCL phase. This fact strongly affects the local mechanical properties of the PCL phase and consequently of the final mechanical properties of investigated nanocomposite. The average roughness (R_a), calculated using AFM height images was different for unmodified and modified M70PLA blend. R_a of neat M70PLA blend was around 21 nm and R_a of M70PLA3HA was about 53 nm. The increase of the average roughness for the blend reinforced with nHA confirmed the incorporation of the nanofillers.

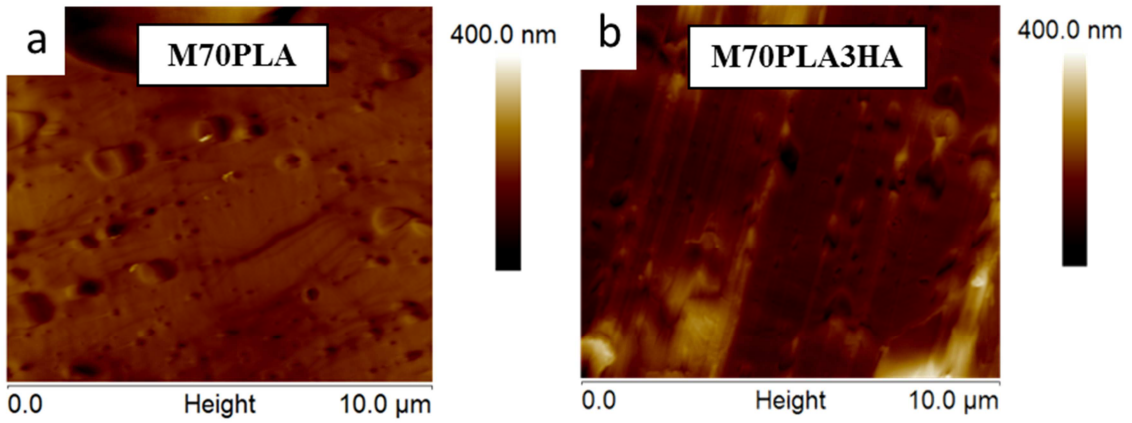

Fig. 8. AFM height images of a) M70PLA and b) M70PLA3HA.

From the analysis of the QNM properties, thus comparing the unmodified M70PLA blend with the corresponding 3 wt % nHA nanocomposite, it can be easily distinguished that the local elastic modulus of PCL-rich separated phase change drastically with the addition of nHA. This fact is evidenced from both the contrast images reported in **Fig. 9** and from the analysis of their corresponding profiles.

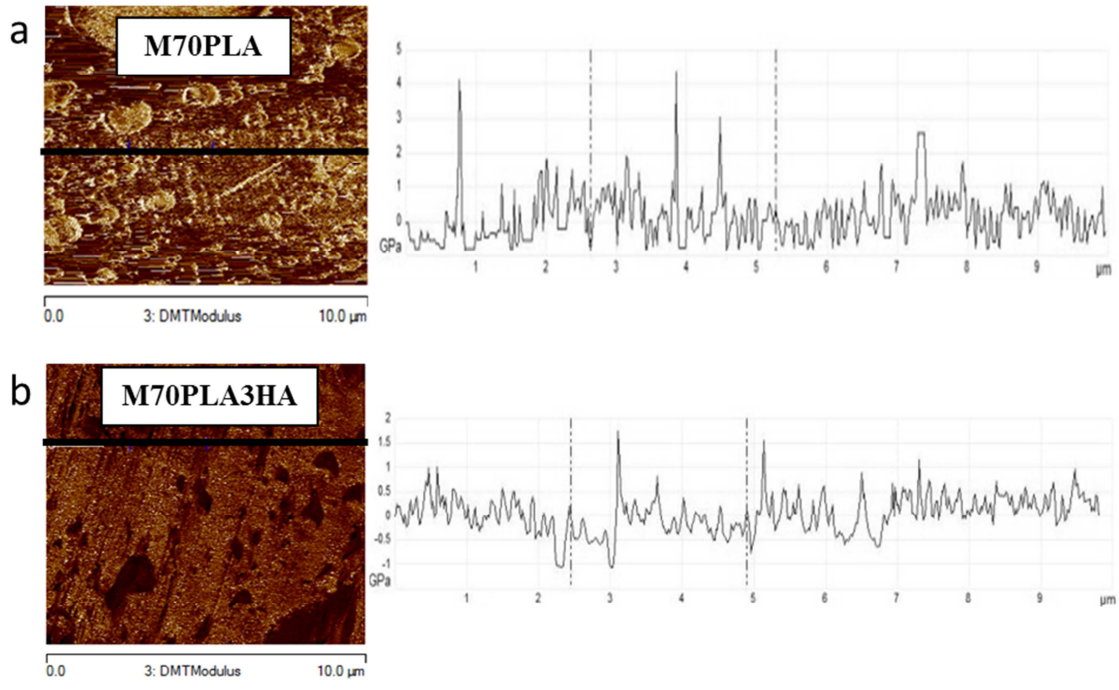

Fig. 9. Quantitative nanomechanical properties obtained by AFM and their corresponding profile for a) M70PLA and b) M70PLA3HA.

Moreover, taking into account that the brighter zone indicates a higher modulus than the darker ones, the modulus ranges from 2.5 to 1.8 GPa. Additionally, it should be pointed out that those significant changes in local elastic modulus occurred for PCL-rich phase

did not affect the average elastic modulus, extracted from PeakForce QNM elastic modulus images of 10 µm x 10µm, of the reinforced and neat M70PLA blends being around 3 GPa for both materials.

Finally, the addition of the 3 wt % of nHA to the polymeric blend affects the adhesion between the separated phases as can be clearly seen in the AFM adhesion images reported in **Fig. 10**.

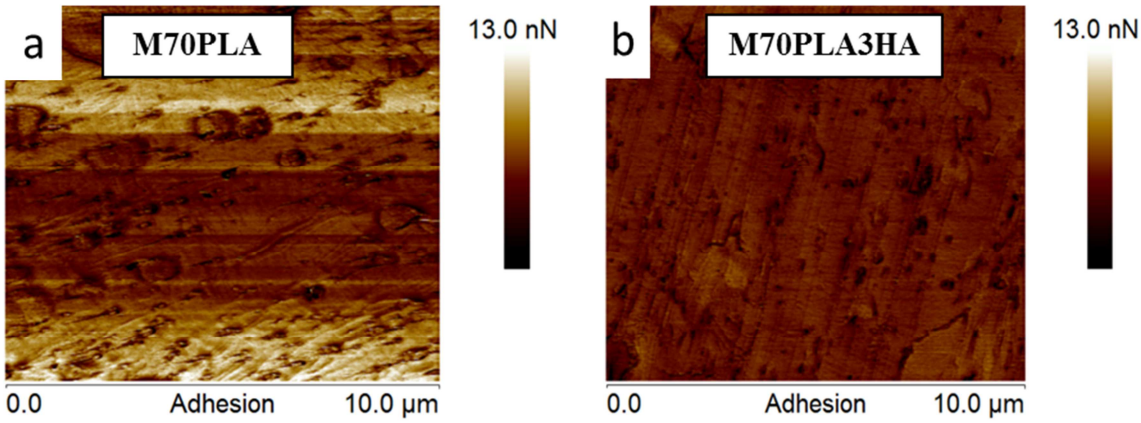

Fig. 10. AFM adhesion images for a) M70PLA and b) M70PLA3HA.

The adhesion of the macro-separated PCL-rich phase changed from 5 nN for M70PLA blend to 10 nN for blend reinforced with 3 wt % nHA. Simultaneously, the adhesion of the matrix remained unchanged. In addition, it seems that when the nHA has been added to the matrix, the "empty" interface between the two separated phases is more evident. This result is in agreement with the SEM images.

Therefore, once correlated the phase-separation microstructure to the micro and macro properties of the nanocomposites, and also studied their thermal and mechanical response, it is easier to perform the thermally-activated shape memory analysis being able to well identify the parameters required for this study. In particular, as it was previously described, a transition temperature closed to the melting temperature of PCL was applied thus considering that in our system, PLA acts as fix phase while crystalline PCL is the switching segment. The digital photographs of **Fig. 11** correspond to M70PLA1HA, as example of the visual appearance of the thermally-activated shape memory process. Firstly, the sample was heated at 55 ºC and deformed to the desired shape. Then it was cooled down reaching the deformed shape reported in **Fig. 11**. Heating again at 55 ºC, the crystalline PCL melts and the sample recovers their initial shape as it is clearly shown in the photograph sequences of **Fig. 11**.

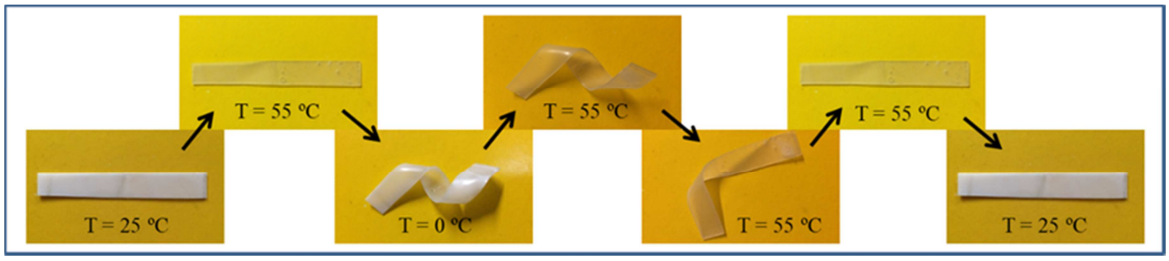

Fig. 11. Thermally-activated shape memory effect of M70PLA1HA. The images show the fixing of the temporary shape and the recovery of the initial shape from the temporary state by heating application.

Shape memory properties of all the samples were studied by DMTA. The elongation applied, ε_m, was 50 % and the switching temperature was 55 ºC. The programming step was designed with a uniaxial stretching at 55 ºC, followed by a fast quenching of the stretched state at 0 ºC. The stretched state was maintained after quenching and subsequent removal of the stress at 0 ºC. **Fig. 12** presents the evolution of strain, stress, and temperature during the dual-shape memory programming step and the consequent free-strain recovery under continuous heating condition at 3 ºC/min, with a recovery time of 30 minutes, for PLA/PCL neat blend and its nanocomposites. The reinforcing effect of nHA can be observed thus considering the stress applied to stretch the specimen, from 1.2 MPa (**Fig. 12.a**) for the neat blend to 1.9 MPa (**Fig. 12.b** and **c**) for a low content of nHA, 0.5 and 1 wt %, while for M70PLA3HA this stress value decrease reaching the same value of the neat blend, that is 1.2 MPa (**Fig. 12.d**). Moreover, it is worth noting that 55 ºC is the exact switching temperature of these materials. In fact, the sample did not change its shape until 55 ºC has been reached and that only when the isothermal ramp started, the specimen recovery process begun. In **Fig. 13** the shape memory results are reported in 3D diagrams of the thermo-mechanical cycles performed. In this Figure it is possible to clearly observe the recover step during the thermo-mechanical cycle and the stability until 55 ºC. However, from both the 2D and the 3D thermo-mechanical diagrams it is visually clear the excellent ability of the both blend and its nanocomposites to fix the temporary shape as well as to recover its initial shape.

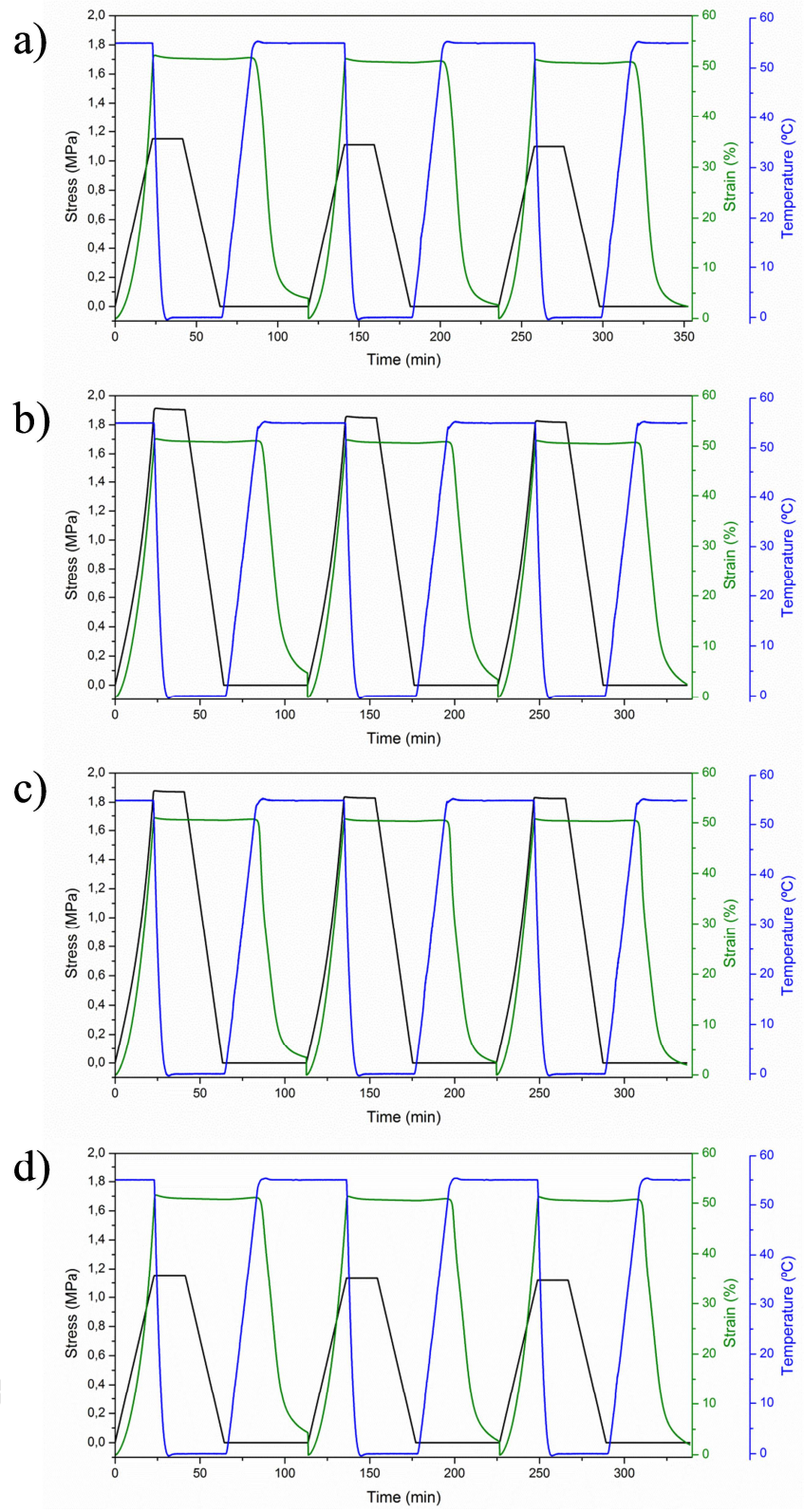

Fig. 12. Evolution of stress, strain, and temperature during three consecutive shape memory cycles for: a) M70PLA, b) M70PLA0.5HA, c) M70PLA1HA and d) M70PLA3HA.

The values of the R_r and the R_f for all the thermo-mechanical cycles are summarized in **Table 2**, confirming the excellent ability to fix the temporary shape of these materials, with R_f higher than 99 % for each cycle.

Table 2. Values of R_r and the R_f for all the samples.

Sample	**R_r (%)**			**R_f (%)**		
Cycle	*1*	*2*	*3*	*1*	*2*	*3*
M70PLA	92	95	95	99	99	99
M70PLA0.5HA	90	93	95	99	99	99
M70PLA1HA	95	95	96	100	100	100
M70PLA3HA	91	95	96	99	99	99

Also the ability to recover the initial shape was very good. $R_{r,}$ in fact, was very high during the first cycle, more than 90 %, and increased until values about 96 % after the third thermo-mechanical cycle. Slightly higher values were obtained for the nanocomposites with 1 and 3 wt % of nHA. Therefore, it is important to note that the addition of nHA did not affect the good response of the neat matrix to fix the temporary shape, showing in each case values higher than 99 % as well as to recovery its permanent shape keeping constant the R_r values after the first cycle with values higher than 96 % for the nanocomposites. This fact could be important thus considering the final application field of shape memory materials. In fact, thus adding small amount of nHA we are able to improve the stiffness of the nanocomposites at the actuation temperature without affecting their ability to both fix their temporary shape and recover their initial shape.

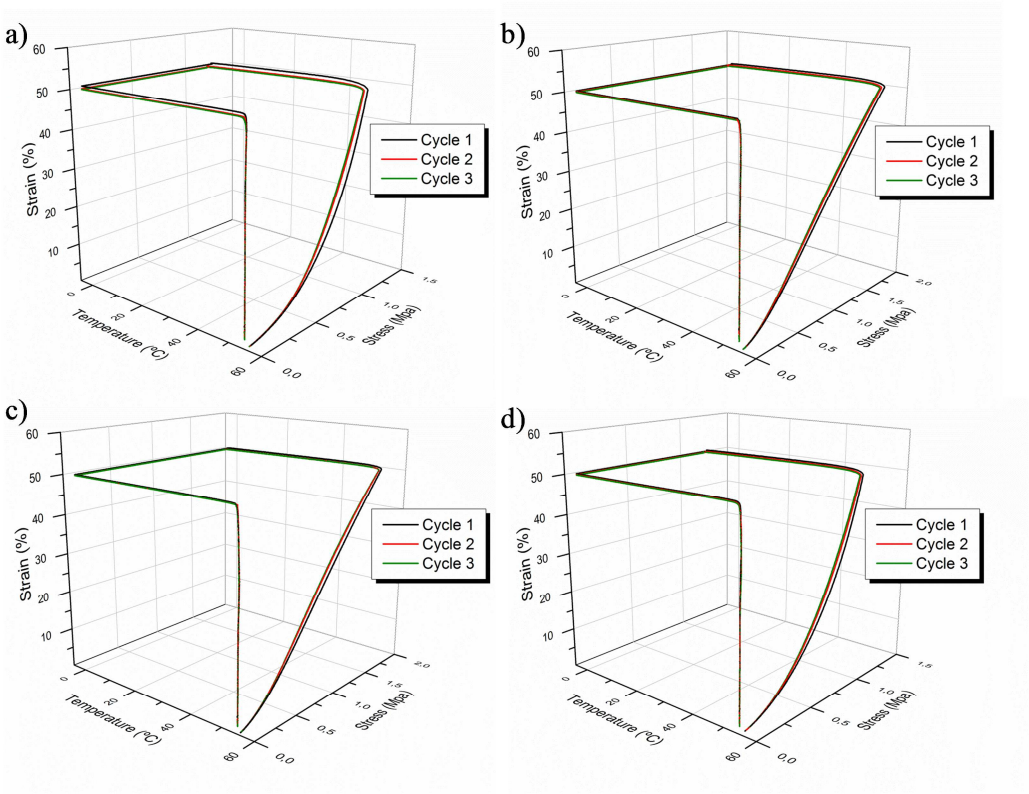

Fig. 13. 3D Thermo-mechanical cycles performed at 55 ºC for: a) M70PLA, b) M70PLA0.5HA, c) M70PLA1HA and d) M70PLA3HA.

As a final study, PLA/PCL blends and their nHA reinforced nanocomposites were disintegrated under composting conditions at laboratory scale-level in order to confirm their biodegradability as a sustainable end-life option. The visual appearance of recovered films at different time of disintegration is shown in **Fig. 14**.

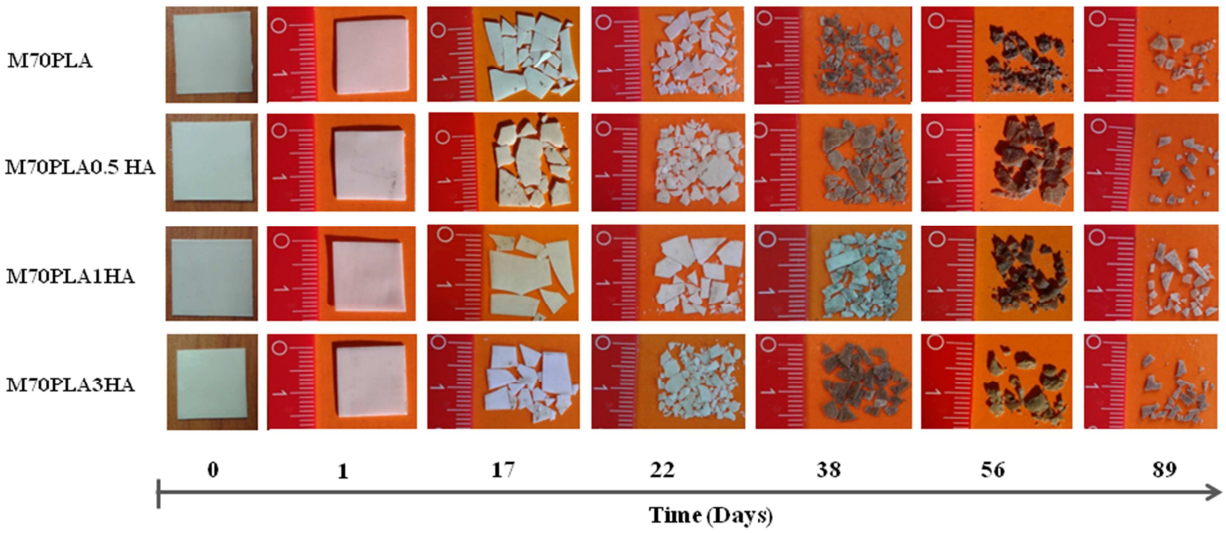

Fig. 14. Visual appearance of disintegrated PLA/PCL blends and its nanocomposites under composting conditions.

During composting, the recovered materials gradually changed their color increasing their opacity, giving evidence that the hydrolytic degradation process is taking place [47]. The films disintegrability was also evaluated in terms of mass loss as a function of time by using the Boltzmann equation to calculate the half-maximal degradation (t_{50}). The disintegrability curves are shown in **Fig. 15** and it is clear that the presence of nHA slowed down the overall disintegration process. For a deep analysis, the surface morphological changes of neat PLA/PCL blend and its nanocomposites before and after composting were followed by SEM (**Fig. 16**). As it can be seen in **Fig. 16.a**, M70PLA exhibited a regular and smooth surface before composting compared with that of the nanocomposites that showed more roughness features (**Fig. 16.d**, **g** and **j**). As previously obtained also by AFM analysis. After 17 days under compost the films became breakable and small pieces of films were recovered (**Fig. 14**), while then at 22 days the degradation process went faster, mainly for M70PLA which lost about 20 % of the initial matter (**Fig. 15**).

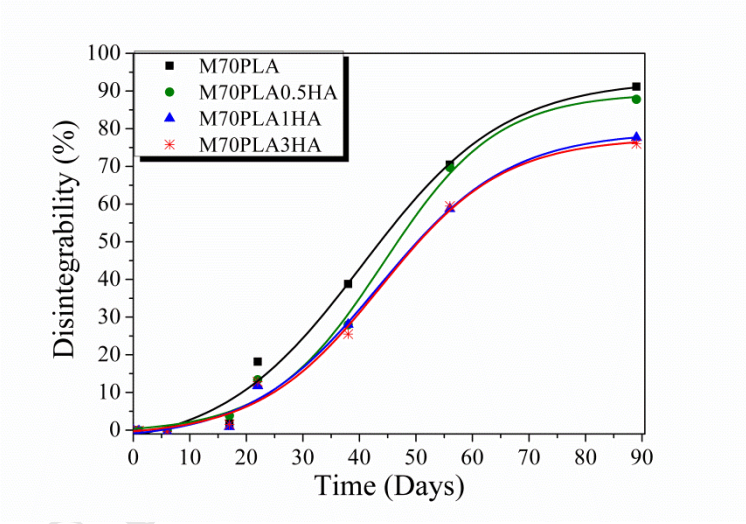

Fig. 15. Disintegrability of PLA/PCL blend and its nanocomposites as a function of time.

It is known that the disintegration process in PLA/PCL blends is faster for PLA than for PCL [10], because of the disintegration in composting of polymer blends starts in the more amorphous component of the polymeric matrix [47]. It has been reported that the disintegration in compost of neat PLA films (~200 µm) takes less than one month [17], while the disintegration of PCL films (~200 µm) requires between 40 and 75 days [10]. In fact, neat PLA matrix in 4 weeks virtually disappeared as it was reported in our previous work [17], thus, at this stage mostly PCL matrix is expected in the blend. The

half-maximal degradation (t_{50}) of M70PLA blend was at about 40 days and this blend reached the goal of disintegrability test (90 % of disintegration [35]) in 90 days. The end of the disintegrability test was considered when pristine M70PLA was totally disintegrated, that is 90 days in composting. After 22 days of the degradation process, it was clear that the nanocomposites resulted more resistant to microorganisms attack (**Fig. 14**). This result was confirmed by SEM observations, where evident signs of surface erosion with some fractures were present in all blends (**Fig. 16.b**, **e**, **h** and **k**), however particularly pristine M70PLA presents some voids of different sizes (**Fig. 16.b**). These findings can be related with the compatibilizer effect of nHA between PLA and PCL, which is reinforcing the PCL/PLA blend, and thus protecting the polymer matrix from the water and microorganisms attack. Accordingly, the rate of disintegration under compost conditions was longer for nanocomposites with respect to the M70PLA (t_{50} = 40.5 days), which showed increasing values of half-maximal degradation with increasing amount of nHA being M70PLA0.5HA t_{50} equal to 44.2 days, M70PLA1HA t_{50} equal to 43.5 days and M70PLA3HA t_{50} equal to 43.7 days. Later than 38 days it is more evident that the nHA was delaying the disintegration process (**Fig. 15**).

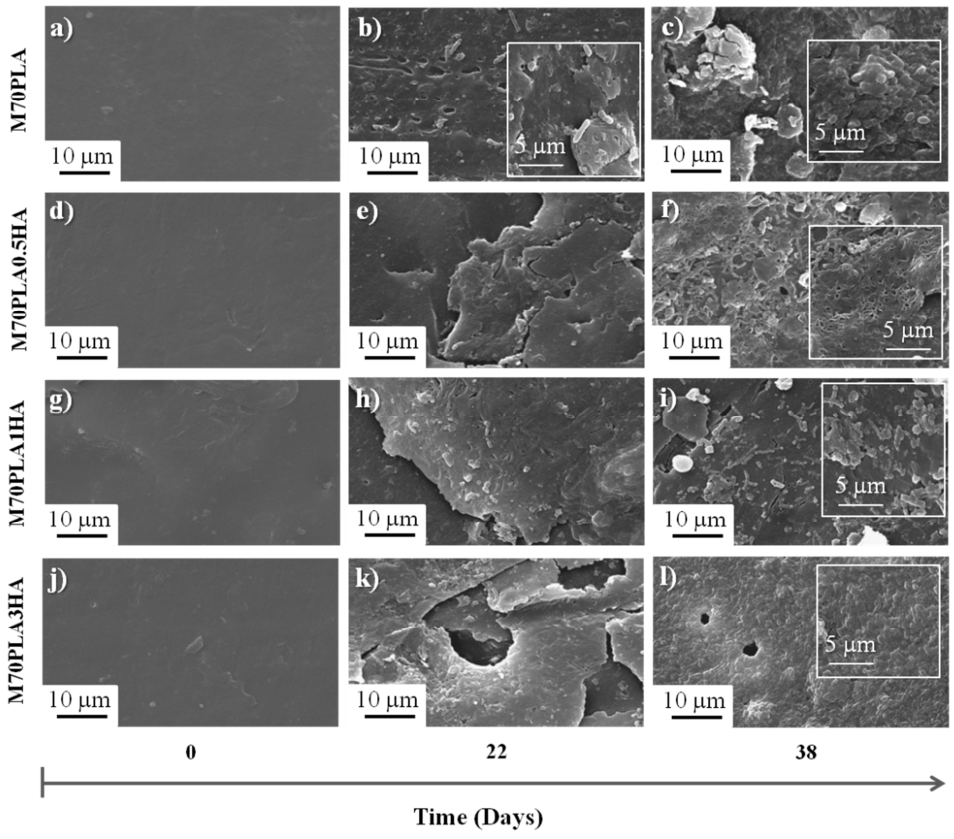

Fig. 16. SEM observations (2500x) of a-c) M70PLA and the nanocomposites d-f) M70PLA0.5HA, g-i) M70PLA1HA and j-k) M70PLA3HA before and after different days of disintegration under composting.

Considering that at this stage the polymeric matrix is mostly PCL, it is suggesting a preferential interaction of the nHA with the PCL than with PLA matrix in the blend, confirming the previous results obtain by PeakForce QNM analysis. These results is also in agreement with previous results were a polyurethane based on PLA and PCL block co-polymers was reinforced with nHA and the nanofiller showed preferential interaction with the PCL-rich phase of the PU matrix [31]. SEM micrographs (**Fig. 16.c**, **f**, **i** and **l**) showed deep signs of disintegration after 38 testing days, and they were particularly notorious M70PLA were some spherical PCL domains are observed (see insert **Fig. 16.c**).

Finally, in order to corroborate the biodegradable nature of the developed nanocomposites the disintegration phenomenon was studied by infrared spectroscopy. The FTIR spectra of M70PLA and its nanocomposite with the higher amount of nHA used (M70PLA3HA) at different degradation times are shown in **Fig. 17.a** and **b**, respectively. The carbonyl band becomes broader at the early disintegration stage of 6 days owing to an increase of the carboxylic end groups in the polymer chain during the hydrolytic degradation, as also previously observed [48]. Moreover, the intensity of carbonyl PCL shoulder increased at this time in M70PLA in **Fig. 17.a**, while it considerably increased for the nanocomposites, as it shown as in **Fig. 17.b** for M70PLA3HA. This different behavior suggests that nHA is mainly protecting the PCL matrix from the water attack. At 22 days, the intensity of carbonyl band increased in both, PLA/PCL blend and its nanocomposites, because of at this stage it is also taking place the disintegration of PCL. The loss of PCL produced the materials toughening which turn into breakable PLA/PCL blends in good agreement with the visual aspect of the films (**Fig. 14**) as well as the SEM observations (**Fig. 16.b**, **e**, **h** and **k**). However, in M70PLA the PLA carbonyl intensity was higher than that of the more crystalline carbonyl group of PCL (**Fig. 17.a**), showing that the disintegration of PLA matrix goes faster. At 38 days, the PCL carbonyl band intensity increased since, at this time, PLA matrix is probably totally disintegrated and additionally the disintegration of PCL is promoted. In nanocomposites the intensity of both carbonyl groups remains constant at 22 days and their intensities simultaneously increased at 38 days. Around 1600 cm^{-1}

appears a broad band, corresponding to the formation of carboxylate ions at the chain ends as a consequence of the hydrolytic degradation, which intensity augmented as the composting time increase, as previously reported [49].

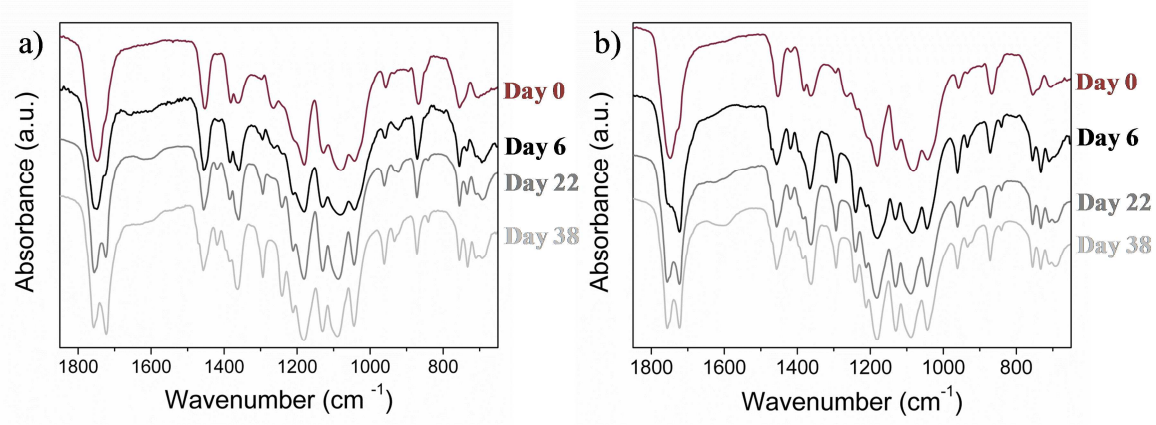

Fig. 17. Infrared spectra of a) M70PLA and b) M70PLA3HA nanocomposite before and after different time of disintegration under composting.

4. Conclusions

The effect of the addition of small amounts of nHA (0.5, 1 and 3 wt %) in a PLA/PCL blend was studied in term of thermally-activated shape memory response. Thermal and mechanical analysis of the nanocomposites has been performed and compared with the neat matrix, not neglecting that phase separation is a key-factor when working with polymeric blends and strongly influenced the macro-properties of the materials. For this reason a deep study on their morphology has been performed by AFM, SEM, FTIR and confocal Raman spectroscopy confirming the phase separation of homopolymers showing a preferential interaction of nHA with the PCL-rich phase. This result is also confirmed by disintegration in compost condition experiments. The presence of nHA slowed down the overall disintegration process mainly showing preference for the PCL-rich phase. Moreover, for all nanocomposites a good dispersion was achieved. In addition, the quantitative nanomechanical analysis performed with PeakForce QNM demonstrates that when the nHA has been added to the matrix, the “empty” interface between the two separated phases is more evident, in good agreement with SEM images. Mechanical properties, for all the nanocomposites, increased in terms of elastic modulus, revealing the expected reinforcement effect even at low concentrations. On the contrary, the thermal properties were not specially affected by the addition of nHA at the studied concentrations. Therefore, the thermally-activated shape memory

response of the nanocomposites was not affected by the addition of nHA in term of transition temperature required and also excellent values for both strain recovery ratio and strain fixity ratio, higher than 95 % and 99 %, respectively has been obtained. Consequently, this study presents new biodegradable materials with excellent thermally-activated shape memory properties, easy to processes by common used processing techniques on the industry level, with enhanced mechanical properties without changing the thermal behavior, useful for their advanced thermally-activated shape memory applications. Additionally, the disintegrability test under composting condition at lab scale, confirmed the biodegradable character of these nanocomposites which can be useful in different areas such as biomedicine or food packaging.

ACKNOWLEDGEMENTS

Authors thank the Spanish Ministry of Economy, Industry and Competitiveness, MINEICO, (MAT2017-88123-P) and the Regional Government of Madrid (S2013/MIT-2862) for the economic support. M.P.A. and L.P. acknowledge the "Juan de la Cierva" (FJCI-2014-20630) and "Ramon y Cajal" (RYC-2014-15595) contracts from the MINEICO, respectively. The authors also thanks CSIC for the I-Link project (I-Link1149).

REFERENCES

[1] P.H.C. Camargo, K.G. Satyanarayana, F. Wypych, Nanocomposites: Synthesis, structure, properties and new application opportunities, Mat. Res. 12(1) (2009) 1-39.

[2] V. Sessini, M.P. Arrieta, J.M. Kenny, L. Peponi, Processing of edible films based on nanoreinforced gelatinized starch, Polym. Degrad. Stab., 2016;132:157-68

[3] L. Yu, K. Dean, L. Li, Polymer blends and composites from renewable resources, Prog. Polym. Sci. 31(6) (2006) 576-602.

[4] R. Rendón-Villalobos, A. Ortíz-Sánchez, E. Tovar-Sánchez, E. Flores-Huicochea, The Role of Biopolymers in Obtaining Environmentally Friendly Materials. In: Poletto M, editor. Composites from Renewable and Sustainable Materials. Rijeka: InTech; 2016. p. Ch. 08.

[5] M.P. Arrieta, M.d.M. Castro-López, E. Rayón, L.F. Barral-Losada, J.M. López-Vilariño, J. López, M.V. González-Rodríguez, Plasticized Poly(lactic acid)–

Poly(hydroxybutyrate) (PLA–PHB) Blends Incorporated with Catechin Intended for Active Food-Packaging Applications, J. Agric. Food. Chem. 62(41) (2014) 10170-10180.

[6] A.J.R. Lasprilla, G.A.R. Martinez, B.H. Lunelli, A.L. Jardini, R.M. Filho, Poly-lactic acid synthesis for application in biomedical devices - A review, Biotechnol. Adv. 30(1) (2012) 321-328.

[7] H. Seyednejad, A.H. Ghassemi, C.F. Van Nostrum, T. Vermonden, W.E. Hennink, Functional aliphatic polyesters for biomedical and pharmaceutical applications, J. Controlled Release 152(1) (2011) 168-176.

[8] R. Auras, B. Harte, S. Selke, An overview of polylactides as packaging materials, Macromol. Biosci. 4(9) (2004) 835-864.

[9] I. Navarro-Baena, A. Marcos-Fernández, A. Fernández-Torres, J.M. Kenny, L. Peponi, Synthesis of PLLA-b-PCL-b-PLLA linear tri-block copolymers and their corresponding poly(ester-urethane)s: Effect of the molecular weight on their crystallisation and mechanical properties, RSC Adv. 4(17) (2014) 8510-8524.

[10] J.M. Ferri, O. Fenollar, A. Jorda-Vilaplana, D. García-Sanoguera, R. Balart, Effect of miscibility on mechanical and thermal properties of poly(lactic acid)/ polycaprolactone blends, Polym. Int. 65(4) (2016) 453-463.

[11] V. Guarino, F. Causa, P. Taddei, M. di Foggia, G. Ciapetti, D. Martini, C. Fagnano, N. Baldini, L. Ambrosio, Polylactic acid fibre-reinforced polycaprolactone scaffolds for bone tissue engineering, Biomaterials 29(27) (2008) 3662-3670.

[12] V. Mittal, T. Akhtar, G. Luckachan, N. Matsko, PLA, TPS and PCL binary and ternary blends: structural characterization and time-dependent morphological changes, Colloid. Polym. Sci. 293(2) (2015) 573-585.

[13] L. Peponi, I. Navarro-Baena, A. Sonseca, E. Gimenez, A. Marcos-Fernandez, J.M. Kenny, Synthesis and characterization of PCL-PLLA polyurethane with shape memory behavior, Eur. Polym. J. 49(4) (2013) 893-903.

[14] Y. Shen, W. Sun, K.J. Zhu, Z. Shen, Regulation of biodegradability and drug release behavior of aliphatic polyesters by blending, J. Biomed. Mater. Res. 50(4) (2000) 528-535.

[15] M.P. Arrieta, V. Sessini, L. Peponi, Biodegradable poly(ester-urethane) incorporated with catechin with shape memory and antioxidant activity for food packaging, Eur. Polym. J. 94(Supplement C) (2017) 111-124.

[16] D. Wu, Y. Zhang, M. Zhang, W. Zhou, Phase behavior and its viscoelastic response of polylactide/poly (ε-caprolactone) blend, Eur. Polym. J. 44(7) (2008) 2171-2183.

[17] I. Navarro-Baena, V. Sessini, F. Dominici, L. Torre, J.M. Kenny, L. Peponi, Design of biodegradable blends based on PLA and PCL: From morphological, thermal and mechanical studies to shape memory behavior, Polym. Degrad. Stab. 132 (2016) 97-108.

[18] A.S. Olalla, V. Sessini, E.G. Torres, L. Peponi, Chapter 9 - Smart Nanocellulose Composites With Shape-Memory Behavior, Multifunctional Polymeric Nanocomposites Based on Cellulosic Reinforcements, William Andrew Publishing 2016, pp. 277-312.

[19] V. Sessini, J.M. Raquez, G. Lo Re, R. Mincheva, J.M. Kenny, P. Dubois, L. Peponi, Multiresponsive Shape Memory Blends and Nanocomposites Based on Starch, ACS Appl. Mater. Interfaces 8(30) (2016) 19197-19201.

[20] V. Sessini, M.P. Arrieta, A. Fernández-Torres, L. Peponi, Humidity-activated shape memory effect on plasticized starch-based biomaterials, Carbohydr. Polym. 179(Supplement C) (2018) 93-99.

[21] A. Lendlein, Shape-memory polymers, Springer 2010.

[22] L. Peponi, I. Navarro-Baena, J.M. Kenny, Shape memory polymers: Properties, synthesis and applications, Smart Polymers and their Applications 2014, pp. 204-236.

[23] H.Q. Dong, L.J. Liu, Y.Y. Li, Shape-memory behavior of poly (L-lactide)/poly (ε-caprolactone) blends, Advanced Materials Research, Trans Tech Publ, 2011, pp. 171-174.

[24] L. Peponi, D. Puglia, L. Torre, L. Valentini, J.M. Kenny, Processing of nanostructured polymers and advanced polymeric based nanocomposites, Mater. Sci. Eng., R 85 (2014) 1-46.

[25] L. Peponi, L. Valentini, L. Torre, I. Mondragon, J.M. Kenny, Surfactant assisted selective confinement of carbon nanotubes functionalized with octadecylamine in a poly (styrene-b-isoprene-b-styrene) block copolymer matrix, Carbon 47(10) (2009) 2474-2480.

[26] I. Navarro-Baena, J.M. Kenny, L. Peponi, Thermally-activated shape memory behaviour of bionanocomposites reinforced with cellulose nanocrystals, Cellulose 21(6) (2014) 4231-4246.

[27] F.K. Molavi, I. Ghasemi, M. Messori, M. Esfandeh, Nanocomposites based on poly (l-lactide)/poly (ε-caprolactone) blends with triple-shape memory behavior: Effect of the incorporation of graphene nanoplatelets (GNps), Compos. Sci. Technol. 151 (2017) 219-227.

[28] J. Venkatesan, S.K. Kim, Nano-hydroxyapatite composite biomaterials for bone tissue engineering - A review, J. Biomed. Nanotechnol. 10(10) (2014) 3124-3140.

[29] A. Sonseca, L. Peponi, O. Sahuquillo, J.M. Kenny, E. Giménez, Electrospinning of biodegradable polylactide/hydroxyapatite nanofibers: Study on the morphology, crystallinity structure and thermal stability, Polym. Degrad. Stab. 97(10) (2012) 2052-2059.

[30] J. Kaur, M.L. Shofner, Surface Area Effects in Hydroxyapatite/Poly(ε-caprolactone) Nanocomposites, Macromol. Chem. Phys. 210(8) (2009) 677-688.

[31] I. Navarro-Baena, M.P. Arrieta, A. Sonseca, L. Torre, D. López, E. Giménez, J.M. Kenny, L. Peponi, Biodegradable nanocomposites based on poly(ester-urethane) and nanosized hydroxyapatite: Plastificant and reinforcement effects, Polym. Degrad. Stab. 121 (2015) 171-179.

[32] V. Sessini, Raquez, J.M., Lourdin, D., Maigret, J.E., Kenny, J.M., Dubois, P., Peponi, L., Humidity-activated Shape Memory Effects on Thermoplastic Starch/EVA Blends and Their Compatibilized Nanocomposites, Macromol. Chem. Phys. 218 (24) (2017) 1700388.

[33] L. Peponi, I. Navarro-Baena, J.E. Báez, J.M. Kenny, A. Marcos-Fernández, Effect of the molecular weight on the crystallinity of PCL-b-PLLA di-block copolymers, Polymer 53(21) (2012) 4561-4568.

[34] B. ISO, 37: 2011 Rubber, vulcanized or thermoplastic—Determination of tensile stress-strain properties, British Standards Institution (BSI), London (2011).

[35] UNE-EN-ISO., 20200. Determination of the degree of disintegration of plastic materials under simulated composting conditions in a laboratory-scale test, 2016.

[36] M.P. Arrieta, E. Fortunati, F. Dominici, J. López, J.M. Kenny, Bionanocomposite films based on plasticized PLA–PHB/cellulose nanocrystal blends, Carbohydr. Polym. 121 (2015) 265-275.

[37] K. Kesenci, L. Fambri, C. Migliaresi, E. Piskin, Preparation and properties of poly(L-lactide)/hydroxyapatite composites, J. Biomater. Sci., Polym. Ed. 11(6) (2000) 617-632.

[38] L.H. Leung, H.E. Naguib, Viscoelastic properties of poly(ε-caprolactone) - hydroxyapatite micro- and nano-composites, Polym. Adv. Technol. 24(2) (2013) 144-150.

[39] A. Rezaei, M. Mohammadi, In vitro study of hydroxyapatite/polycaprolactone (HA/PCL) nanocomposite synthesized by an in situ sol–gel process, Materials Science and Engineering: C 33(1) (2013) 390-396.

[40] X. Li, S. Zhang, X. Zhang, S. Xie, G. Zhao, L. Zhang, Biocompatibility and physicochemical characteristics of poly (Ɛ-caprolactone)/poly (lactide-co-glycolide)/nano-hydroxyapatite composite scaffolds for bone tissue engineering, Materials & Design 114 (2017) 149-160.

[41] M. Sadat-Shojai, M.-T. Khorasani, E. Dinpanah-Khoshdargi, A. Jamshidi, Synthesis methods for nanosized hydroxyapatite with diverse structures, Acta biomaterialia 9(8) (2013) 7591-7621.

[42] N. López-Rodríguez, A. López-Arraiza, E. Meaurio, J.R. Sarasua, Crystallization, morphology, and mechanical behavior of polylactide/poly(ε-caprolactone) blends, Polym. Eng. Sci. 46(9) (2006) 1299-1308.

[43] J. Odent, P. Leclère, J.-M. Raquez, P. Dubois, Toughening of polylactide by tailoring phase-morphology with P [CL-co-LA] random copolyesters as biodegradable impact modifiers, Eur. Polym. J. 49(4) (2013) 914-922.

[44] L. Peponi, A. Tercjak, J. Gutierrez, M. Cardinali, I. Mondragon, L. Valentini, J.M. Kenny, Mapping of carbon nanotubes in the polystyrene domains of a polystyrene-b-polyisoprene-b-polystyrene block copolymer matrix using electrostatic force microscopy, Carbon 48(9) (2010) 2590-2595.

[45] L. Peponi, A. Tercjak, L. Torre, J.M. Kenny, I. Mondragon, Morphological analysis of self-assembled SIS block copolymer matrices containing silver nanoparticles, Compos. Sci. Technol. 68(7) (2008) 1631-1636.

[46] A. Tercjak, J. Gutierrez, C. Ocando, L. Peponi, I. Mondragon, Thermoresponsive inorganic/organic hybrids based on conductive TiO 2 nanoparticles embedded in poly (styrene-b-ethylene oxide) block copolymer dispersed liquid crystals, Acta Mater. 57(15) (2009) 4624-4631.

[47] M.P. Arrieta, J. López, E. Rayón, A. Jiménez, Disintegrability under composting conditions of plasticized PLA–PHB blends, Polym. Degrad. Stab. 108 (2014) 307-318.

[48] M.P. Arrieta, E. Fortunati, F. Dominici, E. Rayón, J. López, J.M. Kenny, PLA-PHB/cellulose based films: Mechanical, barrier and disintegration properties, Polym. Degrad. Stab. 107 (2014) 139-149.

[49] M.P. Arrieta, J. López, D. López, J.M. Kenny, L. Peponi, Effect of chitosan and catechin addition on the structural, thermal, mechanical and disintegration properties of plasticized electrospun PLA-PHB biocomposites, Polym. Degrad. Stab. 132 (2016) 145-156.

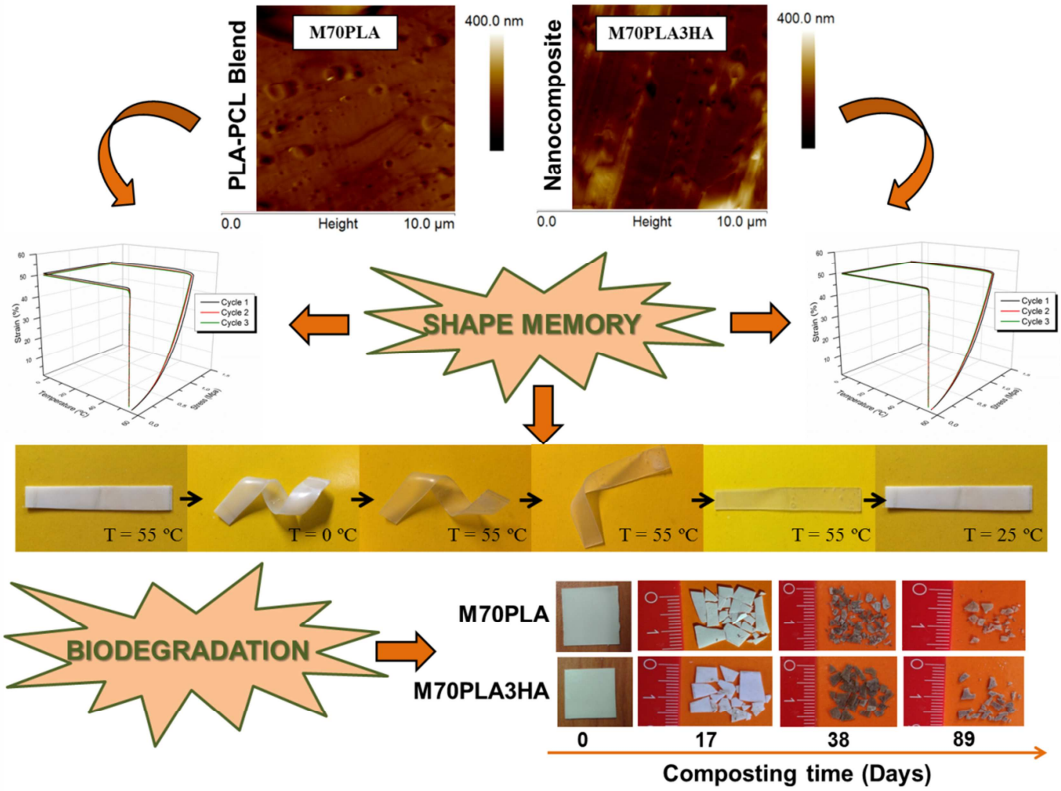

Highlights

- Processing of biodegradable PLA/PCL blend
- PLA/PCL blend reinforced with nano hydroxyapatite
- Thermally-activated shape memory

GRAPHICAL ABSTRACT